Engineering Structures 244 (2021) 112745

Contents lists available at ScienceDirect

Engineering Structures

journal homepage: www.elsevier.com/locate/engstruct

A multi-scale framework for probabilistic structural analysis of PSC girders considering pit corrosion of prestressing wires

Jaebeom Lee [a], Young-Joo Lee [a,*], Chang-Su Shim [b,*]

[a] Department of Urban and Environmental Engineering, Ulsan National Institute of Science and Technology (UNIST), Ulsan 44919, Republic of Korea
[b] School of Civil and Environmental Engineering, Urban Design and Studies, Chung-Ang University, Seoul 06974, Republic of Korea

ARTICLE INFO

Keywords:
Corrosion
Finite element model
Probabilistic analysis
Surrogate model
Prestressed concrete bridge

ABSTRACT

Many standards and studies have emphasized the importance of considering various uncertainty factors of material properties and corrosion in assessing the structural performance of bridges. In such an analysis, however, high computational cost is a major issue because a probabilistic structural analysis requires multiple structural analyses. In this study, an efficient framework for constructing a probabilistic structural analysis model is proposed. First, a surrogate model is constructed using Gaussian process regression for the given structural analysis model. Next, random samples of model inputs and structural responses, which are assumed to be correlated non-Gaussian random variables, are generated based on the Cholesky decomposition and Morgenstern model. Finally, the statistical properties of structural responses are derived by a goodness-of-fit test; hence, they can be considered as probabilistic inputs for an upper-scale model in the form of random variables. This three-step process can be introduced accumulatively from the lower-scale to upper-scale models about a structure; accordingly, it is termed as a multi-scale framework for probabilistic structural analysis. The proposed framework was applied to construct probabilistic models for prestressed concrete (PSC) girders with corroded prestressing wires, and the probabilistic prediction results for the ultimate load and displacement showed a good agreement with the experimental data.

1. Introduction

Predicting the performance of a bridge is a challenging task, because it requires analyzing the performance of structural members (e.g., girders and piers) and their interactions. Moreover, a structural member such as a PSC girder can also be modeled as a complex structural system and its structural analysis can be complicated because it further consists of smaller components such as tendons (i.e., bundles of multiple strands of twisted prestressing wires), concrete beam, and reinforcement bars. In addition, prestressing wires may suffer from corrosion. Although the pit corrosion of prestressing wires may significantly affect the behavior of a PSC bridge, it is extremely difficult to consider every details of corroded wires in a full-scale bridge model. Many researchers have endeavored to develop physics-based models for solving the aforementioned problems, and several studies have formulated numerical models to analyze the effects of corrosion at local-level components (such as prestressing wires and reinforcement bars) on the global-level responses of a bridge or its major structural members. For example, Xu and Wang (2015) developed and verified a finite element (FE) model for steel plates considering pit corrosion [1]. Biondini and Vergani (2015) presented a three-dimensional FE model for a deteriorated reinforced concrete (RC) beam considering corrosion [2]. Li et al. (2017) developed a model for the pitting damage of prestressing steel strands [3]. Guo et al. (2011) performed FE analysis considering corrosion, creep, and shrinkage in PSC girder bridges [4].

Meanwhile, various aleatory and epistemic uncertainty factors exist in assessing the structural safety of corroded bridges that may result in a numerical gap between the prediction model and experimental results. To this end, several standards and studies have emphasized the use of a probabilistic approach to bridge safety assessment (e.g., AASHTO LRFD 2017 [5]). Cho and Kim (2008) constructed an FE model to estimate the probability density function for the vertical and horizontal deflections of a suspension bridge during construction [6]. Huang et al. (2014) suggested a probabilistic structural analysis model to estimate the load–displacement relationship of an RC bridge [7]. Liu and Zhang (2017) presented a new method for establishing a probabilistic baseline of an FE model considering changes in temperature [8]. Yang (2007) proposed a probabilistic analysis method for assessing the effects of

* Corresponding authors.
E-mail addresses: jblee@unist.ac.kr (J. Lee), ylee@unist.ac.kr (Y.-J. Lee), csshim@cau.ac.kr (C.-S. Shim).

https://doi.org/10.1016/j.engstruct.2021.112745
Received 27 January 2021; Received in revised form 18 May 2021; Accepted 18 June 2021
Available online 30 June 2021
0141-0296/© 2021 The Authors. Published by Elsevier Ltd. This is an open access article under the CC BY-NC-ND license (http://creativecommons.org/licenses/by-nc-nd/4.0/).

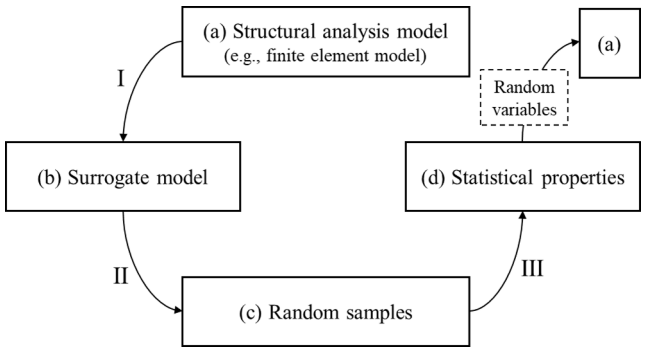

Fig. 1. Overview of probabilistic multi-scale structural analysis framework.

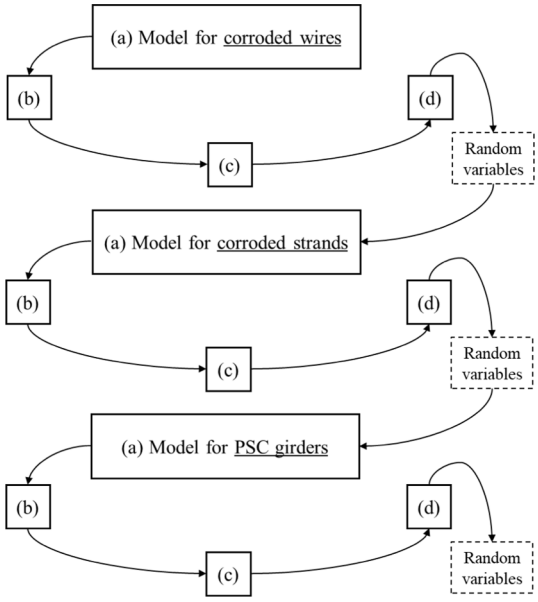

Fig. 2. Application example of probabilistic multi-scale structural analysis framework.

concrete creep and drying shrinkage on PSC box girder bridges [9]. Lee et al. (2016) recommended a reliability analysis platform employing an FE model to consider the uniform corrosion of steel [10] that was utilized by Kim et al. (2017) to derive the flood fragility curves for a corroded RC bridge [11].

However, the probabilistic analysis about a structure requires multiple structural analyses, which increases the computational cost; thus, a structural analysis model needs to be constructed in a way that the computational cost of structural analysis can be reduced properly. To achieve this, Petrolo et al. (2012) studied the reduction of model dimensions without significant losses of accuracy [12]. Toi et al. (1994) and Bažant et al. (2007) developed a mesh size calibration method for FE models to minimize the computational cost without substantially reducing accuracy [13,14]. Alternatively, several studies using FE models have adopted a finer mesh size for important structural members and a coarser mesh size for less critical ones [15,16]. Other researchers have developed surrogate models. Depending on the research field, this approach is also called metamodeling or response surface modeling, and several civil engineering problems have been solved by building such a surrogate model. Qin et al. (2018) suggested a kriging method based on machine learning to update an FE model where a genetic algorithm was used [17], and Wu et al. (2018) introduced a kriging method with Latin hypercube sampling [18]. Zhang and Wu (2019) used the kriging method to construct a surrogate model for the seismic vulnerability analysis of RC bridges [19].

However, the above methods for reducing the computational cost of structural analysis have rarely been applied to corroded PSC bridges. In practice, detailed modeling of the geometrically complex corroded tendons, concrete parts, and reinforcement bars, which are the components of the PSC girders and bridges, can improve the model accuracy but the computational cost. Therefore, an efficient method of reducing the computational cost without a significant reduction in accuracy needs to be developed. In this study, an efficient framework for the probabilistic structural analysis of PSC girders reflecting the corrosion of local structural components (such as prestressing wires) is suggested to solve this problem. The proposed framework is based on a robust fitting of probabilistic distributions to lower the computational cost without significantly reducing the accuracy of the analysis results.

2. Probabilistic Multi-Scale structural analysis framework

This study aims to construct a structural analysis model for corroded PSC girders considering various uncertainty variables, such as material properties, corrosion rate, and corrosion size. The proposed framework for building a probabilistic analysis model is a cyclic process, as depicted in Fig. 1. Once a structural analysis model ((a)) for a lower-scale structural component is developed, a surrogate model ((b)) is constructed based on the given model to reduce the computational cost (I). Using this computationally efficient model, random samples of model inputs and the associated structural responses ((c)) are generated (II). Next, the statistical properties of structural responses for given model inputs ((d)) are derived by a goodness-of-fit test (III). Consequently, the structural analysis results of the lower-scale model can be considered as simple random variables in an upper-scale model.

Because of this cyclic applicability, the multi-scale terminology can be introduced to build the structural analysis model of a complicated structural system. For instance, the structural analysis results for the corroded wires can be converted as random variables and introduced in the analysis model of the corroded strands, which is the upper scale model as shown in Fig. 2. Similarly, the analysis results for the corroded strands can be considered as random variables, which are the analysis model inputs for the PSC girders. Because the probabilistic properties of random variables contain information about the lower scale components, such as corrosion, material properties, and geometric characteristics, the lower scale components can be modeled as a simple element in the upper scale model. Therefore, both the accuracy and computational efficiency of the model can be improved using this cyclic process.

2.1. Surrogate model construction

The structural responses (e.g., load–displacement curve) are affected by several uncertainty factors, such as material properties and corrosion size. The effects of these random variables can be accounted for through probabilistic structural analysis, which requires conducting numerous structural analyses of many possible combinations of the values of random variables. However, such an approach can be computationally inefficient when the analysis model has high computational cost. To resolve this, a surrogate model may be constructed [20]. The first step in surrogate model construction is to design experiments. In this study, the central composite design (CCD) method proposed by Myers et al. (2016) was used to preselect the combinations of random variable values for experiments [21] that were then used for structural analyses. The analysis results for the preselected combinations of random variable values are used to construct a non-parametric surrogate model through the Gaussian process regression (GPR), which is a machine learning-based Bayesian regression method. As a stochastic process, the Gaussian process (GP) presumes that every data-set follows multivariate Gaussian distributions, and the GPR is conducted based on this GP assumption [20,22].

Let $\mathbf{D}$ be the matrix of the preselected combinations of random variable values, and $\mathbf{y}_1$ and $\mathbf{y}_2$ be the vectors of the corresponding ultimate

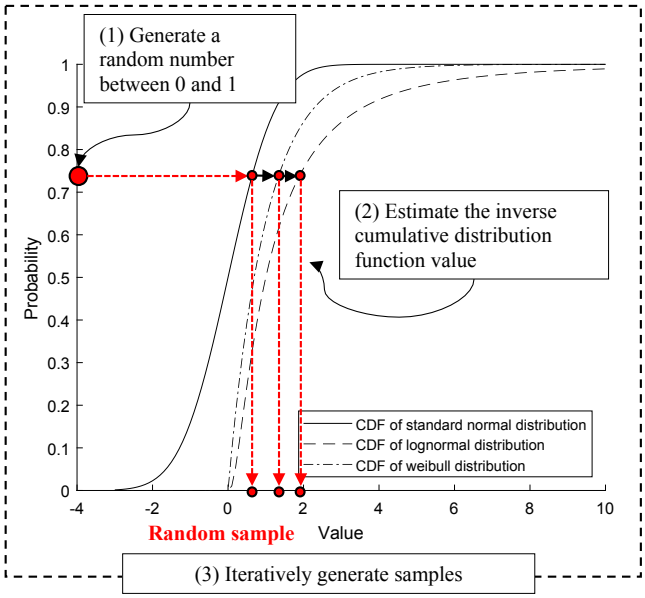

Fig. 3. Sample generation using inverse transform method.

load and displacement obtained from structural analysis, respectively:

$$[\mathbf{y}_1 \quad \mathbf{y}_2] = \left[\begin{bmatrix} y_{1,1} \\ y_{1,2} \\ y_{1,3} \\ \vdots \end{bmatrix} \quad \begin{bmatrix} y_{2,1} \\ y_{2,2} \\ y_{2,3} \\ \vdots \end{bmatrix} \right] = SA\left(\begin{bmatrix} \mathbf{d}_1 \\ \mathbf{d}_2 \\ \mathbf{d}_3 \\ \vdots \end{bmatrix} \right) = SA(\mathbf{D}) \tag{1}$$

where $SA(\cdot)$ is a structural analysis model, and $y_{1,i}$ and $y_{2,i}$ are the analysis results of the ultimate load and displacement for the ith combination of random variable values ($\mathbf{d}_i$), respectively. The GP assumption allows the surrogate models, $\hat{f}_{y_1}(\hat{\mathrm{A}}\cdot)$ and $\hat{f}_{y_2}(\hat{\mathrm{A}}\cdot)$, for the ultimate load (i.e., $\mathbf{y_1}$) and displacement (i.e., $\mathbf{y_2}$) to be derived as multivariate Gaussian variables for a new matrix of random variables, $\mathbf{D}_*$:

$$\begin{pmatrix} \mathbf{y}_1 \\ \hat{f}_{y_1}\left(\mathbf{D}_*, \hat{\theta}_{11}, \hat{\theta}_{12}\right) \end{pmatrix} = N(\mathbf{O}, \Sigma_1) = N\left(\mathbf{O}, \begin{bmatrix} k_1(\mathbf{D},\mathbf{D}) + \sigma_{n_1}^2\mathbf{I} & k_1(\mathbf{D},\mathbf{D}_*) \\ k_1(\mathbf{D}_*,\mathbf{D}) & k_1(\mathbf{D}_*,\mathbf{D}_*) \end{bmatrix}\right) \tag{2}$$

and

$$\begin{pmatrix} \mathbf{y}_2 \\ \hat{f}_{y_2}\left(\mathbf{D}_*, \hat{\theta}_{21}, \hat{\theta}_{22}\right) \end{pmatrix} = N(\mathbf{O}, \Sigma_2) = N\left(\mathbf{O}, \begin{bmatrix} k_2(\mathbf{D},\mathbf{D}) + \sigma_{n_2}^2\mathbf{I} & k_2(\mathbf{D},\mathbf{D}_*) \\ k_2(\mathbf{D}_*,\mathbf{D}) & k_2(\mathbf{D}_*,\mathbf{D}_*) \end{bmatrix}\right) \tag{3}$$

where $\hat{\theta}_{11}$, $\hat{\theta}_{12}$, $\hat{\theta}_{21}$, and $\hat{\theta}_{22}$ are the hyperparameters for the covariance matrices, $\mathbf{\Sigma}_1$ and $\mathbf{\Sigma}_2$; $N(\mathbf{O}, \mathbf{\Sigma}_1)$ and $N(\mathbf{O}, \mathbf{\Sigma}_2)$ denote the multivariate Gaussian distributions with a zero mean matrix (i.e., $\mathbf{O}$); $\mathbf{\Sigma}_1$ and $\mathbf{\Sigma}_2$ are the covariance matrices; $\sigma_{n_1}^2$ and $\sigma_{n_2}^2$ are the data noises; $\mathbf{I}$ is an identity matrix; and $k_1(\cdot,\cdot)$ and $k_2(\cdot,\cdot)$ are the kernel functions [22]. The covariance matrices (i.e., $\mathbf{\Sigma}_1$ and $\mathbf{\Sigma}_2$) can be constructed by using the following kernel functions (i.e., $k_1(\cdot,\cdot)$ and $k_2(\cdot,\cdot)$) for two given input vectors of $\mathbf{d}_1$ and $\mathbf{d}_2$:

$$k_1(\mathbf{d}_1,\mathbf{d}_2) = \hat{\theta}_{11}^2 exp\left(-\frac{1}{2}\frac{\Delta(\mathbf{d}_1,\mathbf{d}_2)}{\hat{\theta}_{12}^2}\right) \tag{4}$$

and

$$k_2(\mathbf{d}_1,\mathbf{d}_2) = \hat{\theta}_{21}^2 exp\left(-\frac{1}{2}\frac{\Delta(\mathbf{d}_1,\mathbf{d}_2)}{\hat{\theta}_{22}^2}\right) \tag{5}$$

where $\Delta(\cdot,\cdot)$ represents the Euclidean distance. These kernel functions

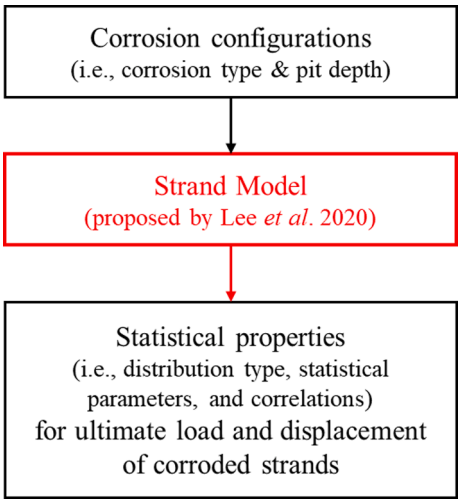

Fig. 5. Inputs and outputs of strand model proposed by Lee et al. (2020) [20].

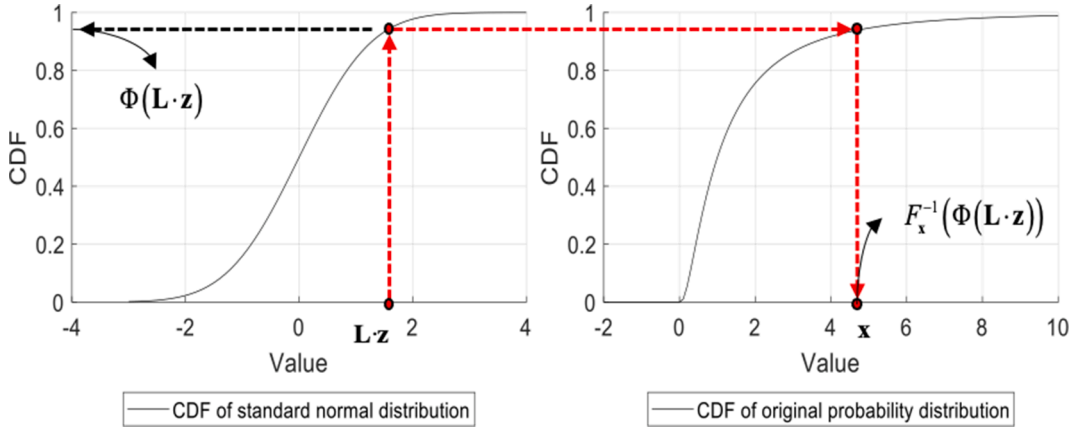

Fig. 4. Coordinate transformation from standard normal random variables to original variables.

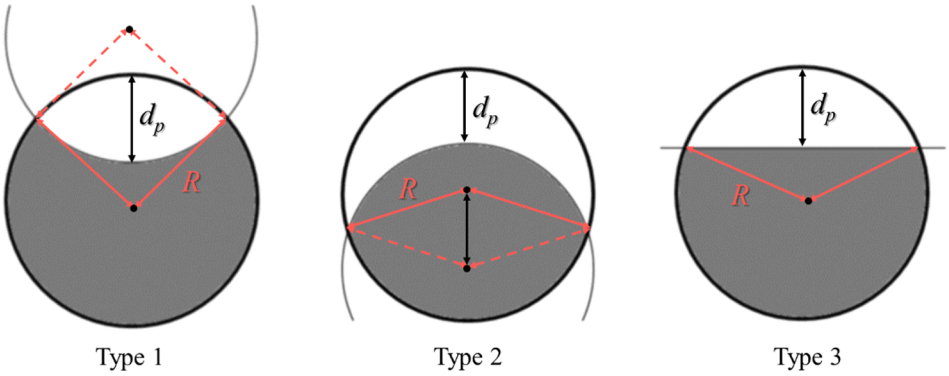

Fig. 6. Three pit types categorized by Jeon et al. (2019) [28] in which white and gray spaces indicate corroded and non-corroded sections, respectively.

Table 1
Corrosion configurations of prestressing strands used for validation.

Strand specimen	Wire	Pit type	Pit depth (mm)
TS1	W0	–	–
	W1	–	–
	W2	–	–
	W3	–	–
	W4	–	–
	W5	–	–
	W6	–	–
TS2	W0	–	–
	W1	–	–
	W2	2	0.03
	W3	2	0.08
	W4	2	0.11
	W5	–	–
	W6	–	–
TS3	W0	–	–
	W1	1	0.70
	W2	1	0.35
	W3	3	0.90
	W4	–	–
	W5	–	–
	W6	–	–
TS4	W0	–	–
	W1	2	0.80
	W2	–	–
	W3	2	0.27
	W4	–	–
	W5	–	–
	W6	–	–

Table 2
Statistical properties derived from strand model.

Strand specimen	Ultimate load	Ultimate displacement	Correlation
TS1	*Weibull* (k = 259,981, λ = 51.0395)	*Normal* (μ = 7.345, σ = 0.588)	−0.2217
TS2	*Weibull* (k = 259,395, λ = 50.0046)	*Normal* (μ = 6.289, σ = 0.313)	−0.1022
TS3	*Weibull* (k = 251,163, λ = 51.1398)	*Normal* (μ = 1.687, σ = 0.209)	0.1828
TS4	*Weibull* (k = 249,371, λ = 50.7502)	*Normal* (μ = 1.504, σ = 0.111)	0.2277

numerically represent the covariance, which is the product of the standard deviation and correlation. In other words, $\widehat{\theta}_{11}$ and $\widehat{\theta}_{21}$ denote the variance, and $\widehat{\theta}_{12}$ and $\widehat{\theta}_{22}$ are the length scale factors for estimating the correlation between two inputs. To find the best combinations for the kernel hyperparameters, the conditional probabilities of outputs $\mathbf{y}_1$ and $\mathbf{y}_2$ given input $\mathbf{D}$ can be used:

$$p_1(\mathbf{y}_1|\mathbf{D}) = \frac{1}{(2\pi)^{\frac{N_\mathbf{D}}{2}}\left|k_1(\mathbf{D},\mathbf{D}) + \sigma_{n_1}^2\mathbf{I}\right|^{\frac{1}{2}}} \cdot exp\left(-\frac{1}{2}\mathbf{y}_1^T\left(k_1(\mathbf{D},\mathbf{D}) + \sigma_{n_1}^2\mathbf{I}\right)\mathbf{y}_1\right) \tag{6}$$

and

$$p_2(\mathbf{y}_2|\mathbf{D}) = \frac{1}{(2\pi)^{\frac{N_\mathbf{D}}{2}}\left|k_2(\mathbf{D},\mathbf{D}) + \sigma_{n_2}^2\mathbf{I}\right|^{\frac{1}{2}}} \cdot exp\left(-\frac{1}{2}\mathbf{y}_2^T\left(k_2(\mathbf{D},\mathbf{D}) + \sigma_{n_2}^2\mathbf{I}\right)\mathbf{y}_2\right) \tag{7}$$

where $N_\mathbf{D}$ is the number of preselected combinations of random variable values. The best hyperparameters for properly designing the covariance are found by solving the following optimization problems:

$$\left[\widehat{\theta}_{11,best}, \widehat{\theta}_{12,best}\right] = \underset{\widehat{\theta}_{11},\widehat{\theta}_{12}}{\text{argmax}} p_1(\mathbf{y}_1|\mathbf{D}) \tag{8}$$

and

$$\left[\widehat{\theta}_{21,best}, \widehat{\theta}_{22,best}\right] = \underset{\widehat{\theta}_{11},\widehat{\theta}_{12}}{\text{argmax}} p_2(\mathbf{y}_2|\mathbf{D}) \tag{9}$$

2.2. Sample generation for correlated non-Gaussian random variables

As described in Fig. 1, the next step is the sample generation of model inputs and the associated structural responses. Once a surrogate model is constructed, structural responses for the given model inputs can be obtained efficiently using the surrogate model. Therefore, the random sample generation of model inputs naturally leads to the sample generation of corresponding structural responses. However, in many structural problems, random variables are non-Gaussian and correlated, making the foregoing difficult.

When single random variable is of interest, its samples can be generated simply using the inverse transform method [23] which is also known as inverse transform sampling and illustrated in Fig. 3: a random number is generated using the uniform distribution function between 0 and 1, and the inverse cumulative distribution function (CDF) at the generated random number is estimated. The inverse transform method can be used to generate random samples even though the random variable of interest is non-Gaussian, and these two steps can then be iterated as many times as necessary. In an actual structural problem, however, there must be multiple random variables (e.g., the ultimate load and displacement of a corroded strand, which need to be the inputs of the structural analysis model for a PSC girder), and they are often known to be correlated. In such an occasion, the inverse transform method is not applicable as it is.

To deal with multiple correlated random variables in a reliability

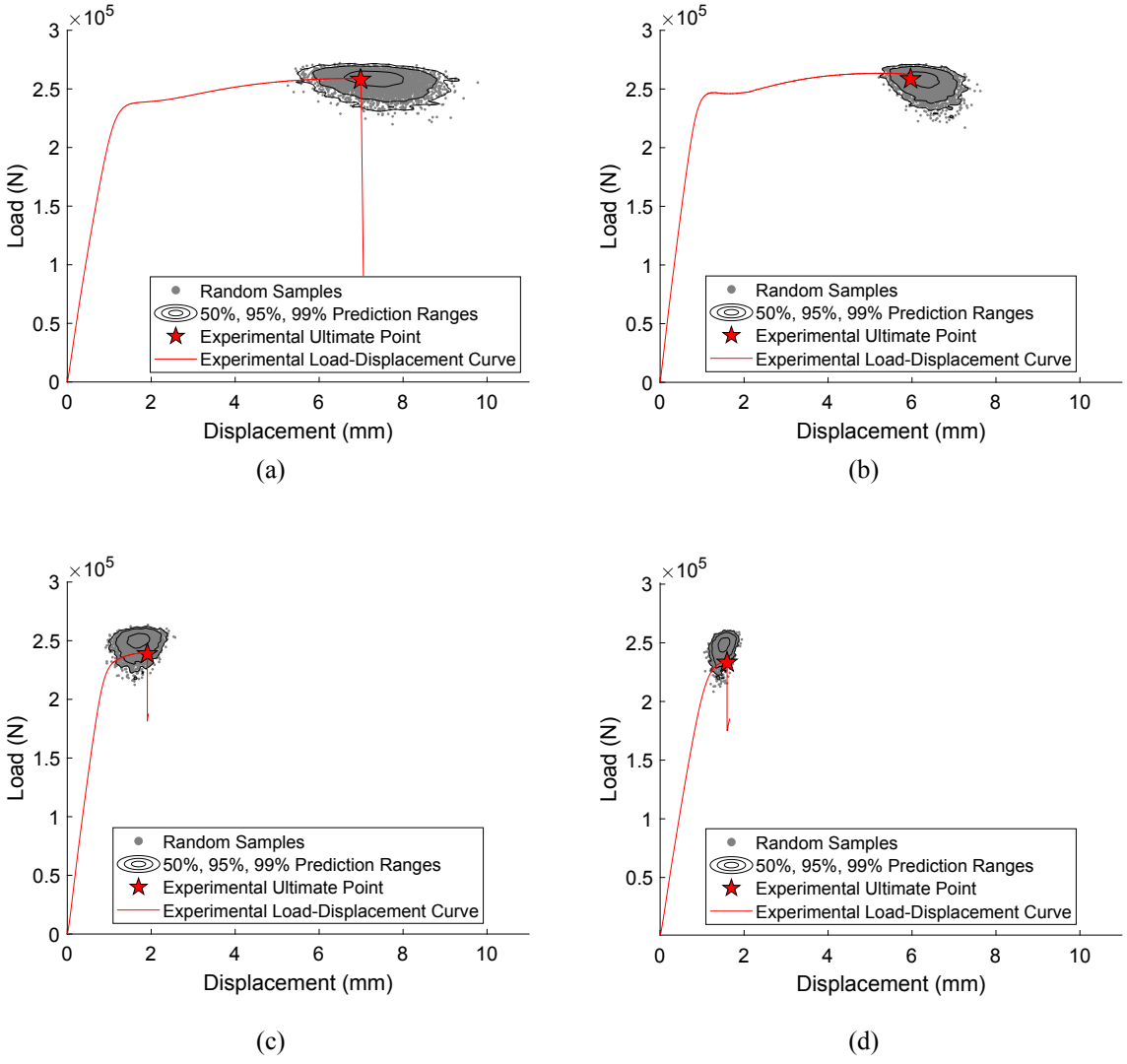

Fig. 7. Probabilistic prediction ranges for ultimate load and displacement of corroded strands: (a) TS1, (b) TS2, (c) TS3, and (d) TS4.

Table 3
Probabilistic model versus experimental results of ultimate load.

Strand specimen	50% prediction range (N)	95% prediction range (N)	99% prediction range (N)	Experimental result (N)
TS1	251,900–264,800	239,000–270,400	229,700–271,700	258,000
TS2	251,300–265,000	236,300–268,800	230,000–271,800	258,500
TS3	244,000–255,800	231,000–259,300	219,200–261,700	238,700
TS4	241,700–254,200	229,300–258,700	221,300–259,900	233,300

Table 4
Probabilistic model versus experimental results of ultimate displacement.

Strand specimen	50% prediction range (mm)	95% prediction range (mm)	99% prediction range (mm)	Experimental result (mm)
TS1	6.61–8.02	5.71–8.82	5.41–9.22	6.99
TS2	5.87–6.67	5.49–7.11	5.17–7.37	5.97
TS3	1.01–1.96	1.12–2.25	1.45–2.40	1.91
TS4	1.17–1.65	1.25–1.81	1.39–1.87	1.59

analysis, Liu and Der Kiureghian (1986) introduced the Cholesky decomposition, which decomposes a positive-definite matrix into the product of the lower and upper triangular matrices [24]. The design correlation matrix, $\mathbf{R}_{design}$, can be decomposed as follows:

$$\mathbf{R}_{design} = \mathbf{L}\cdot\mathbf{L}^T \tag{10}$$

where $\mathbf{L}$ is the lower triangular matrix, and $\mathbf{L}^T$ is its conjugate transpose (i.e., the upper triangular matrix). Then, multiplying the lower triangular matrix of the design correlation matrix and the generated samples based on the multi-variate standard normal distribution (i.e., $\mathbf{z}$) yields the correlation matrix of $\mathbf{R}_{design}$:

$$\mathbf{R}_{\mathbf{L}\cdot\mathbf{z}} = E\left[\mathbf{L}\cdot\mathbf{z}\cdot(\mathbf{L}\cdot\mathbf{z})^T\right] = E\left[\mathbf{L}\cdot\mathbf{z}\cdot\mathbf{z}^T\cdot\mathbf{L}^T\right] = \mathbf{L}\cdot\mathbf{I}\cdot\mathbf{L}^T = \mathbf{R}_{design} \tag{11}$$

This means that the first and second row vectors of $\mathbf{L}\,\mathbf{z}$ are correlated samples following the bi-variate standard normal distribution with the correlation matrix, $\mathbf{R}_{design}$. However, considering the following coordinate transformation shown in Fig. 4:



(a)



(b)

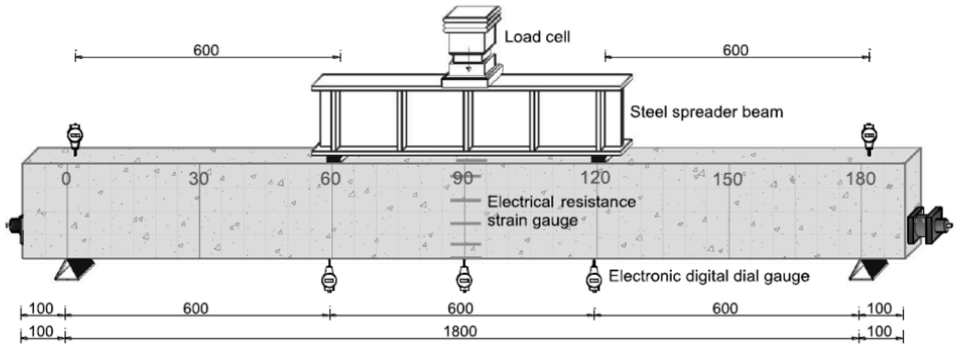

(c)

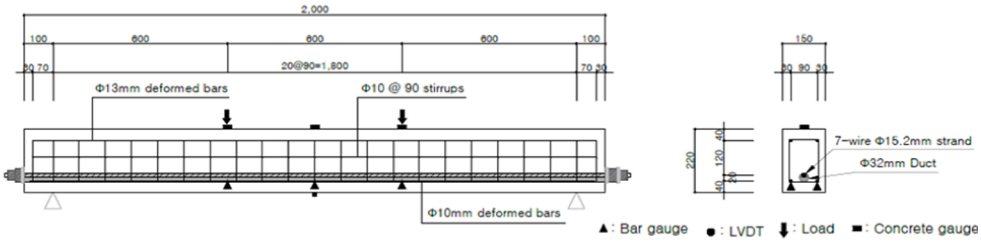

(d)

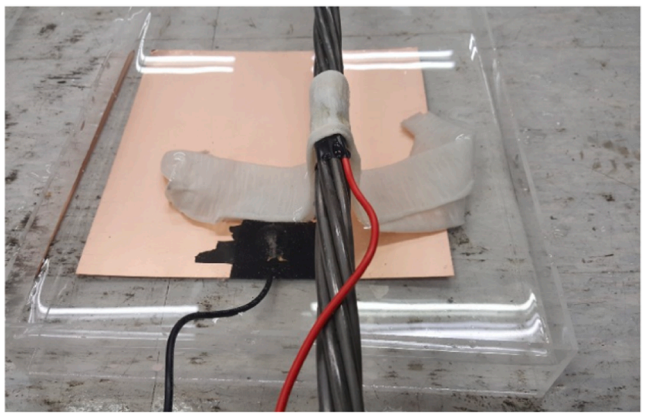

(e)

Fig. 8. Specimen preparation: (a) formwork and sensor installation, (b) tendon precast, (c) bending test setup, (d) PSC girder and sensors, and (e) electrochemical corrosion induction.

Table 5
Corrosion configurations of prestressing strands in girder specimens.

Girder specimen	Strand	Wire	Pit type	Pit depth (mm)	Sectional area (mm^2)
Girder #01	S1	W0	–	0.00	20.89
		W1	–	0.00	19.63
		W2	–	0.00	19.63
		W3	–	0.00	19.63
		W4	–	0.00	19.63
		W5	–	0.00	19.63
		W6	–	0.00	19.63
Girder #02	S1	W0	–	0.00	20.89
		W1	–	0.00	19.63
		W2	3	1.37	15.27
		W3	3	1.23	15.88
		W4	–	0.00	19.63
		W5	3	0.54	18.49
		W6	–	0.00	19.63
Girder #03	S1	W0	–	0.00	20.89
		W1	–	0.00	19.63
		W2	3	1.06	16.60
		W3	3	1.22	15.93
		W4	3	1.14	16.27
		W5	3	0.22	19.33
		W6	–	0.00	19.63

$$\mathbf{x} = F_x^{-1}(\Phi(\mathbf{L}\cdot\mathbf{z})) \tag{12}$$

where $F_{\mathbf{x}}(\cdot)$ is the CDF for the original probability distribution of random variables $\mathbf{x}$, and $\Phi(\cdot)$ is the CDF of the standard normal random variable; the resultant correlation matrix is not the same as $\mathbf{R}_{design}$. When the resultant correlation coefficient matrix is $\mathbf{R}_{resultant}$, the relationship between $\mathbf{R}_{design}$ and $\mathbf{R}_{resultant}$ is given by the Nataf or Morgenstern models summarized by Liu and Der Kiureghian (1986) [24]. Conversely, the correlation in the standard normal space (i.e., $\mathbf{R}_{design}$) can be designed to obtain random samples having the target correlation in the original space; therefore, random samples can be generated for the correlated non-Gaussian distributions. The random samples for the structural analysis inputs generated by this method can be used as inputs for the prebuilt surrogate model to generate the random samples of structural responses.

2.3. Goodness-of-fit test

The next step is a goodness-of-fit test to parameterize the probabilistic analysis results. As aforementioned, similar multi-scale approaches employing surrogate models have been proposed in previous studies, but the surrogate models have been constructed so that the mean or mean and standard deviation of structural responses match the desired values. To obtain more accurate reliability analysis results with an upper-scale structural model, however, a surrogate model needs to be constructed to reflect the probabilistic distribution of a structural component, which is simplified as a random variable, as much as possible. For this purpose, the goodness-of-fit test is used in this study.

According to Ang and Tang (2007), the Anderson–Darling (A–D) test assigns more weight to the tails of the probability density functions (PDFs) of random variables, compared with the Kolmogorov–Smirnov (K–S) test [25]. Structural responses, such as ultimate load and displacement, are related to extreme events that usually occur at the tails of PDFs; thus, the A–D test can be utilized to find the best fit among several probability distributions. The A–D statistics (A^2) is estimated as

$$A^2 = -\sum_{j=1}^{n}\left[\frac{(2j-1)\{lnF_X(x_j) + ln[1-F_X(x_{n+1-j})]\}}{n}\right] - n \tag{13}$$

where x_j is the jth given dataset, n is the number of given datasets, and $F_X(\cdot)$ is the CDF of the tested probability distribution. The tested probability distribution is found to be acceptable when A^2 is less than the critical value (c_α) for a given significance level, α (e.g., 5%). The more details of the A–D test can be found in the study of Ang and Tang (2007) [25]. When passing this goodness-of-fit test, a structural component can be considered as a random variable in an upper-scale model, as described in Fig. 1.

3. Application example: a PSC girder with corroded strands

The proposed method consisting of the three steps (i.e., surrogate modeling, sample generation, and goodness-of-fit test) is applied to a PSC girder with corroded strands. In this structural problem, firstly, the mechanical characteristics of corroded strands are estimated in terms of the ultimate load and displacement. Based on the analysis results, a single tendon consisting of corroded prestressing wires can be simplified into a single random variable while maintaining its probabilistic characteristics. Using the simplified random variable, the ultimate load and displacement of a PSC girder with a corroded tendon can be further estimated. In other words, the proposed multi-scale framework can be applied to predict the ultimate load and displacement of a PSC girder by conducting a two-cycle analysis (i.e., from wire to strand and from strand to girder).

3.1. Prediction of ultimate load and displacement for corroded strands

In a previous study by Lee et al. (2020), the ultimate load and displacement of corroded strands were successfully predicted using a probabilistic approach [20]. The present study reviews the analysis results of Lee et al. (2020) and utilizes these as inputs for the structural analysis model of a PSC girder. Prestressing strands, each of which consists of a core wire and multiple helical wires, are crucial to the performance of PSC bridges. Thus, estimating their strength and ductility is important for proper bridge safety management. The strands, which have uncertainties in material properties, size, and corrosion measurements, are geometrically complex and vulnerable to pit corrosion. Because these factors have to be carefully considered, the model proposed by Lee et al. (2020) for estimating the ultimate load and displacement of corroded strands is used to represent the prestressing strands of a PSC girder [20]. In this study, the corrosion type and pit depth of the most corroded section along the prestressing wires are considered as the input for the strand model (Fig. 5), as adopted in previous studies [26–29]. First, the pit corrosion of a prestressing wire needs to be categorized into three types, as shown in Fig. 6 [28,29]. The white and gray spaces indicate the corroded and non-corroded sections, respectively. Pit types 1 and 2 are modeled by overlapping two circles with the sectional radius (R) and pit depth (d_p), whereas the corrosion area for pit type 3 is designed to be semicircular. However, it is also noteworthy that the introduction of other critical factors such as the shape of the pit along the wire axis may improve the accuracy of the strand model, and the proposed framework is not limited to the introduction of additional factors. The details of the numerical models for the corroded strands can be found in the literature [20,28], and the pit type and depth can be determined through visual inspection and pit depth gauging, respectively. Once the details are entered into the model, the statistical properties (i.e., distribution type, statistical parameters, and correlations) of the ultimate load and displacement of each corroded strand can be derived, considering the uncertainties in material properties, wire size, and measurement error [20].

According to Lee et al. (2020), the ultimate load and displacement of corroded strands follow the two-parametric Weibull and Gaussian distributions, respectively [20]. For instance, the statistical properties for the ultimate load and displacement of a 100-mm diameter non-corroded seven-wire strand (2.58-mm diameter core wire and 2.5-mm diameter helical wires) are ($k = 259{,}981$, $\lambda = 51.04$) and ($\mu = 7.34$, $\sigma = 0.59$) in the Weibull and Gaussian distributions, respectively, with a correlation coefficient of -0.2217. The PDFs of the Weibull (i.e., $f_{weibull}(x)$) and Gaussian (i.e., $f_{Gaussian}(x)$) distributions are as follows:

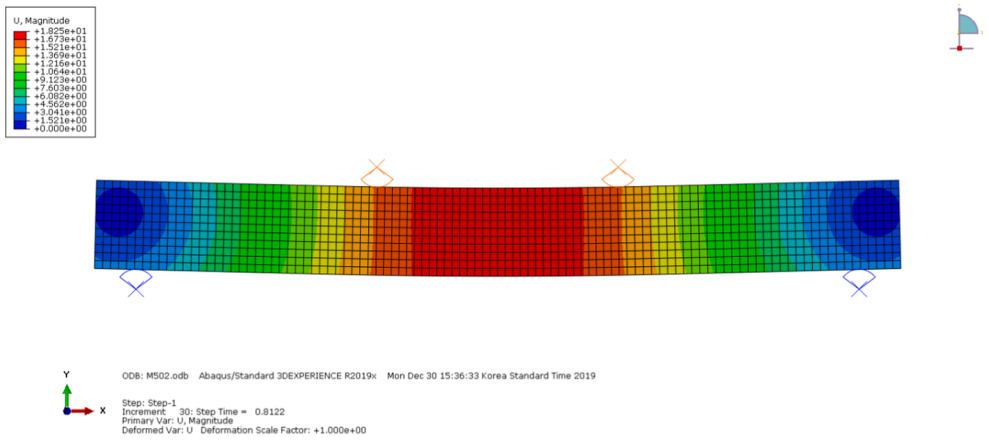

(a)

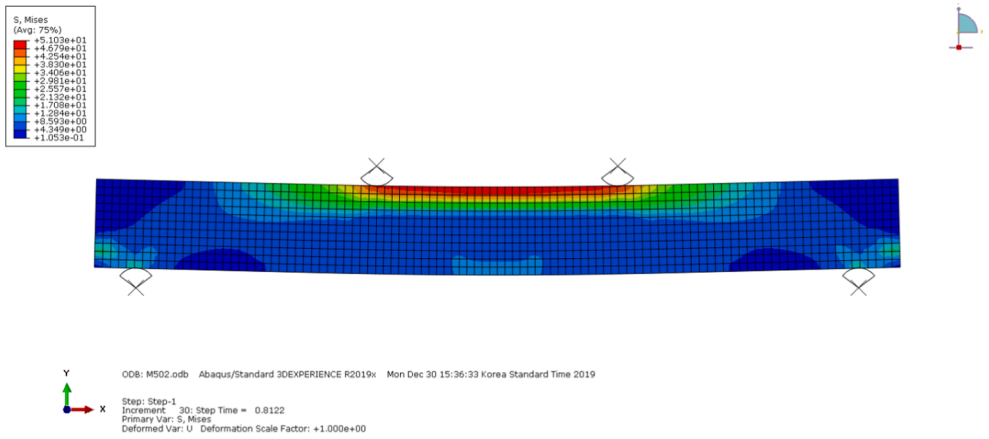

(b)



(c)

Fig. 9. FE models for girders and examples of analysis results: (a) concrete displacement plot, (b) concrete stress plot, and (c) tendon stress plot.

$$f_{weibull}(x) = \begin{cases} \frac{k}{\lambda}\left(\frac{x}{\lambda}\right)^{k-1} e^{-(x/\lambda)^k} & \text{for } x \geq 0 \\ 0 & \text{for } x < 0 \end{cases} \tag{14}$$

and

$$f_{Gaussian}(x) = \frac{1}{\sigma\sqrt{2\pi}} e^{-\frac{1}{2}\left(\frac{x-\mu}{\sigma}\right)^2} \tag{15}$$

In a previous study [28], four specimens (TS1–TS4) of seven-wire strands were collected from an existing bridge in the Republic of Korea and subjected to tensile tests for validation. The radius of each

Table 6
Statistical properties of random variables (Girder #01).

Random variables	Statistical properties	Reference
Ultimate load of strand (N)	*Weibull* (k = 259,981, λ = 51.040)	Lee et al. (2020)
Ultimate displacement of strand (mm)	*Normal* (μ = 7.345, σ = 0.588)	Lee et al. (2020)
Sectional area of strand (mm^2)	*Normal* (μ = 138.74, σ = 2.895)	Lee et al. (2020)
Compressive strength of concrete (f_{cc}) (MPa)	*Normal* (μ = 43.85, σ = 7.893)	Experiment, CEB (1995)
Strain at peak strength of concrete	$\frac{0.7\cdot(f_{cc})^{0.31}}{1000}$	Bae et al. (2016), CEB (1995)
Elastic modulus of concrete (MPa)	$22,000\cdot\left[\frac{(f_{cc}+8)}{10}\right]^{1/3}$	

Table 7
Correlation coefficients among random variables (Girder #01).

Random variables	Ultimate load	Ultimate displacement	Sectional area	Compressive strength
Ultimate load	1.0000	−0.2217	0.0029	0.0000
Ultimate displacement	−0.2217	1.0000	−0.0074	0.0000
Sectional area	0.0029	−0.0074	1.0000	0.0000
Compressive strength	0.0000	0.0000	0.0000	1.0000

Table 8
Statistical properties of random variables (Girder #02).

Random variables	Statistical properties	Reference
Ultimate load of strand (N)	*Weibull* (k = 240,621, λ = 51.138)	Lee et al. (2020)
Ultimate displacement of strand (mm)	*Normal* (μ = 1.212, σ = 0.039)	Lee et al. (2020)
Sectional area of strand (mm^2)	*Normal* (μ = 129.46, σ = 2.794)	Lee et al. (2020)
Compressive strength of concrete (f_{cc}) (MPa)	*Normal* (μ = 43.85, σ = 7.893)	Experiment, CEB (1995)
Strain at peak strength of concrete	$\frac{0.7\cdot(f_{cc})^{0.31}}{1000}$	Bae et al. (2016), CEB (1995)
Elastic modulus of concrete (MPa)	$22,000\cdot\left[\frac{(f_{cc}+8)}{10}\right]^{1/3}$	

Table 9
Correlation coefficients among random variables (Girder #02).

Random variables	Ultimate load	Ultimate displacement	Sectional area	Compressive strength
Ultimate load	1.0000	0.5767	−0.0013	0.0000
Ultimate displacement	0.5767	1.0000	−0.0235	0.0000
Sectional area	−0.0013	−0.0235	1.0000	0.0000
Compressive strength	0.0000	0.0000	0.0000	1.0000

core wire was 2.6 mm, and that of the each of the six surrounding helical wire was 2.5 mm (i.e., the strands had a nominal diameter of 15.2 mm), and the length of each strand was 1000 mm. The strand specimens were loaded using the displacement control method at a speed of 5 mm/min, and failure was assumed to occur when at least one wire was broken. Table 1 summarizes the corrosion configurations at the most corroded section of the specimens, and Table 2 lists the statistical properties estimated from the strand model [20], and the correlation between two variables of B and C (i.e., $\rho_{B,C}$) is calculated as follows:

$$\rho_{B,C} = \frac{E[(B-\mu_B)(C-\mu_C)]}{\sigma_B\sigma_C} \tag{16}$$

Table 10
Statistical properties of random variables (Girder #03).

Random variables	Statistical properties	Reference
Ultimate load of strand (N)	*Weibull* (k = 238,585, λ = 50.986)	Lee et al. (2020)
Ultimate displacement of strand (mm)	*Normal* (μ = 1.228, σ = 0.040)	Lee et al. (2020)
Sectional area of strand (mm^2)	*Normal* (μ = 128.31, σ = 2.847)	Lee et al. (2020)
Compressive strength of concrete (f_{cc}) (MPa)	*Normal* (μ = 43.85, σ = 7.893)	Experiment, CEB (1995)
Strain at peak strength of concrete	$\frac{0.7\cdot(f_{cc})^{0.31}}{1000}$	Bae et al. (2016), CEB (1995)
Elastic modulus of concrete (MPa)	$22,000\cdot\left[\frac{(f_{cc}+8)}{10}\right]^{1/3}$	

Table 11
Correlation coefficients among random variables (Girder #03).

Random variables	Ultimate load	Ultimate displacement	Sectional area	Compressive strength
Ultimate load	1.0000	0.5919	−0.0081	0.0000
Ultimate displacement	0.5919	1.0000	−0.0046	0.0000
Sectional area	−0.0081	−0.0046	1.0000	0.0000
Compressive strength	0.0000	0.0000	0.0000	1.0000

where $E[\ ]$ denotes the expectation, μ_B, μ_C, σ_B and σ_C are the means of B and C and the standard deviations of B and C, respectively. These statistical properties are used to generate 10,000 random samples for the ultimate load and displacement of each specimen; they are plotted as gray dots in Fig. 7. The 50%, 95%, and 99% probabilistic ranges are determined by kernel density estimation [30,31] and plotted as irregular contours. The experimental results of the tensile tests are plotted as red stars.

The failure points of the tested specimens are within the probabilistic prediction ranges, as shown in Fig. 7. This indicates that the mechanical properties of the corroded strands can be represented as correlated Weibull and Gaussian random variables, as recommended by Lee et al. (2020) [20]. For better comparison, Tables 3 and 4 summarize the quantitative results of the predicted mean, prediction ranges, and actual tensile test results for the ultimate load and displacement, respectively. The actual tensile test results were confirmed to be well within the prediction ranges for both the ultimate load and displacement, which quantitatively shows that these statistical properties can represent the ultimate load and displacement of the given corroded prestressing strands. Therefore, the corroded prestressing strands can be modeled as simple line elements, and their mechanical properties can be considered as random variables in the upper-scale model of the PSC girder.

3.2. Prediction of ultimate load and displacement for PSC girder

In this study, three PSC girder specimens (each with a corroded tendon) are prepared as examples, as shown in Fig. 8 [29]. The width, height, and span of the concrete component of each specimen are 150, 220, and 2000 mm, respectively. The sectional area of the non-corroded seven-wire strand is 138.67 mm^2, as shown in Fig. 8(c) and (d). Each of the three specimens has a non-corroded concrete part with compressive strength (f_{cc}) and elastic modulus (E_c) values of 43.85 and 36076.44 MPa, respectively, and the concrete damage, such as crack and spalling, which may coexist with the corrosion on the tendons, was not considered in this study. An electrochemical method was employed to design different corrosion configurations as shown in Fig. 8(e) at the center on the strands (i.e., 900 mm from the support). Girder #01 has a non-corroded strand, and Girders #02 and #03 have corrosion configurations for the most corroded section of the prestressing strands, as

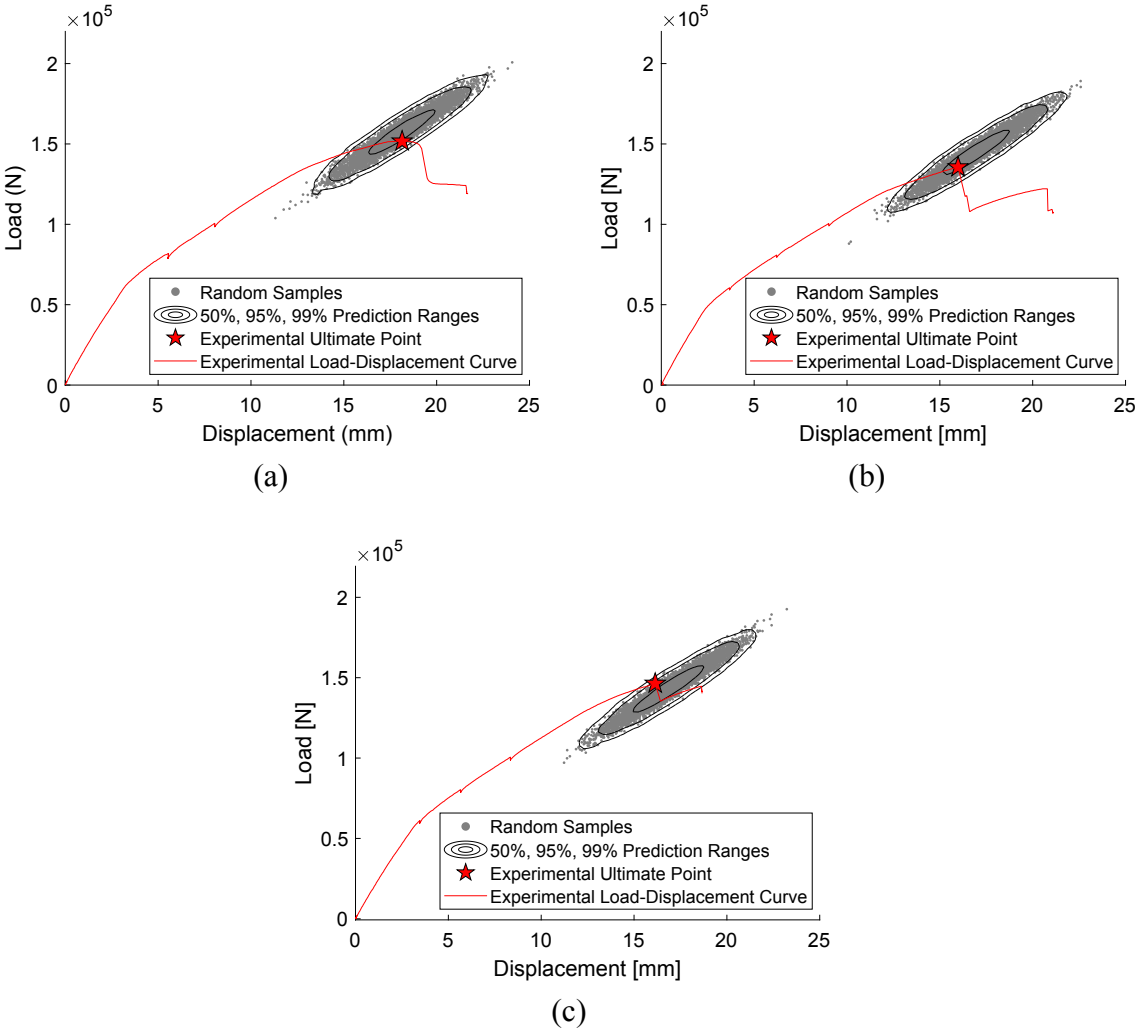

Fig. 10. Probabilistic prediction ranges for ultimate load and displacement of PSC girders: (a) Girder #01, (b) Girder #02, and (c) Girder #03.

Table 12
Probabilistic model versus experimental results for ultimate load.

Girder specimen	50% prediction range (N)	95% prediction range (N)	99% prediction range (N)	Experimental result (N)
Girder #01	142,600–170,600	127,500–185,700	118,900–192,100	151,700
Girder #02	130,700–157,700	115,000–173,400	108,200–180,100	135,600
Girder #03	129,000–156,500	116,200–171,400	105,600–179,900	146,400

Table 13
Probabilistic model versus experimental results for ultimate displacement.

Girder specimen	50% prediction range (mm)	95% prediction range (mm)	99% prediction range (mm)	Experimental result (mm)
Girder #01	16.42–19.82	14.43–21.80	13.30–22.94	18.14
Girder #02	15.10–18.70	13.16–20.65	12.33–21.75	15.95
Girder #03	14.96–18.68	13.10–20.56	12.30–21.36	16.14

Table 14
A–D test results for ultimate load.

Girder specimen	A–D statistics (A^2)				
	Normal	Lognormal	Gamma	Two-parameter Weibull	Three-parameter Weibull
Girder #01	**0.4258**	1.6265	1.1105	1.2647	1.1965
Girder #02	**0.1464**	1.1410	**0.6543**	**0.7370**	1.0705
Girder #03	**0.5113**	**0.4386**	**0.3299**	1.4897	**0.2595**

summarized in Table 5. For example, the strand in Girder #03 has a non-corroded core wire (i.e., W0), and four corroded helical wires with pit type 3.

Four-point bending tests were recently conducted on three PSC girder specimens to analyze the flexural strength of corroded PSC beams deterministically [29]. The tests were performed until either the compressed concrete attained a compressive strain of 0.003 or at least one wire was broken, wherein the vertical deflections were measured using a

Table 15
A–D test results for ultimate displacement.

Girder specimen	A–D statistics (A^2)				
	Normal	Lognormal	Gamma	Two-parameter Weibull	Three-parameter Weibull
Girder #01	**0.7133**	2.5144	1.7947	1.8354	1.3827
Girder #02	**0.4656**	1.7049	1.0918	**0.6143**	1.6751
Girder #03	**0.5373**	**0.5574**	**0.3943**	1.6750	**0.2607**

linear variable differential transformer (LVDT) sensor attached to their mid-spans. The FE models of the PSC girders were constructed separately using ABAQUS, a commercial FE software package, as shown in Fig. 9, and the FE modes are used in this study to perform probabilistic structural analysis. In the FE models, the concrete and strand were modeled as two-dimensional plane and truss elements, respectively. Prestressing strand corrosion was assumed to cause imperfect bonding between the tendon and the surrounding concrete, designed to be debonded. Therefore, the constraint between the location of the corrosion on the strands and the surrounding concrete was modeled as imperfectly bonded, whereas the non-corroded strands were modeled as embedded in the concrete. A concrete damage plasticity model in ABAQUS was adopted to represent the concrete nonlinear stress–strain relationship [32]:

$$\frac{\sigma_c}{f_{cc}} = \frac{\left(1.05 \times E_c \times \frac{0.0238}{f_{cc}}\right) \times \frac{\varepsilon_c}{0.0238} - \left(\frac{\varepsilon_c}{0.0238}\right)^2}{1 + \left(\left(1.05 \times E_c \times \frac{0.0238}{f_{cc}}\right) - 2\right) \times \frac{\varepsilon_c}{0.0238}} \tag{17}$$

where σ_c and ε_c are the concrete stress and strain, respectively. The mechanical properties of the corroded strands for the given corrosion configurations were derived using the strand model [20]. The strands were modeled as simple line elements for the structural analysis of the PSC girders.

Tables 6–11 summarize the statistical properties of the random variables for the given specimens. The ultimate load and displacement of the strands decreased with corrosion, and the concrete compressive strength was the same for every specimen (i.e., all non-corroded). The correlation between the ultimate load and displacement of the strands is naturally close to zero; however, because corrosion simultaneously reduces the ultimate load and displacement, the correlation increases with corrosion.

The probabilistic prediction results for the ultimate load and displacement of the given specimens and experimental bending test results are shown in Fig. 10. To derive the probabilistic ranges, 10,000 random samples are generated for each Girder considering the statistical properties of the random variables that are summarized in Tables 6–11. The small gray dots denote the ten thousands of random samples that have been extracted from the surrogate model, and the three irregular circles represent the 50%, 95%, and 99% prediction ranges that are inferred using the kernel density estimation method. For comparison, the ultimate load and displacement from the actual bending test are plotted as red stars. The failure points of each Girder are within the prediction ranges, indicating that the probabilistic predictions agree with the experimental test results. For better comparison, Tables 12 and 13 summarize the quantitative results of the predicted mean, prediction ranges, and bending test for the ultimate load and displacement, respectively. The actual bending test results are well within the prediction ranges of both the ultimate load and displacement. Therefore, the constructed model is acceptable for estimating the structural responses of the investigated PSC Girders, considering the pit corrosion of the prestressing strands.

In this study, the A–D test was conducted for five probability distributions: normal, lognormal, gamma, two-parameter Weibull, and three-parameter Weibull. Tables 14 and 15 list the cases where $A^2 < c_{5\%}$. Both the ultimate load and displacement best fitted into the normal distributions; the correlations between the ultimate load and displacement for Girders #01, #02, and #03 were estimated to be 0.9612, 0.9688, and 0.9695, respectively. The strain at the peak stress of concrete, known to be proportional to the compressive strength, results in high correlations [33,34]. The given PSC girder specimens were predominantly composed of concrete; thus, the ultimate load and displacement of the PSC girders were estimated to have high correlations.

4. Conclusions

In this study, an efficient multi-scale framework for constructing a probabilistic structural analysis model is proposed. First, a surrogate model is constructed using GPR for the given structural analysis model. Next, random samples of model inputs and the associated structural responses, which are assumed to be correlated non-Gaussian random variables, are generated based on the Cholesky decomposition and Morgenstern model. Finally, the statistical properties of structural responses are derived by a goodness-of-fit test. Consequently, they can be considered as probabilistic inputs for an upper-scale model in the form of random variables. This three-step process can be introduced accumulatively from the lower-scale to the upper-scale models about a structure; accordingly, it has been termed as a multi-scale framework for probabilistic structural analysis. The proposed framework was applied to construct probabilistic models for PSC girders with corroded prestressing wires. The probabilistic prediction results for the ultimate load and displacement were consistent with the experimental data, and the normal distribution best represented the probability distributions of the ultimate load and displacement of the investigated corroded PSC girders. Therefore, the proposed framework can be useful for efficient structural analysis in a probabilistic manner. In addition, it is expected that the proposed framework can be used for constructing efficient probabilistic structural analysis models of PSC girders considering other essential factors, including the modeling methods for different pit corrosion configurations, debonding effects of corrosion, and damage to concrete.

CRediT authorship contribution statement

Jaebeom Lee: Conceptualization, Methodology, Software, Validation, Investigation, Writing - original draft, Writing - review & editing, Visualization. **Young-Joo Lee:** Conceptualization, Methodology, Investigation, Resources, Writing - review & editing, Supervision, Project administration, Funding acquisition. **Chang-Su Shim:** Validation, Investigation, Resources, Writing - review & editing, Project administration, Funding acquisition.

Declaration of Competing Interest

The authors declare that they have no known competing financial interests or personal relationships that could have appeared to influence the work reported in this paper.

Acknowledgment

This research was supported by a grant (21SCIP-B128570-05) from Construction technology research program funded by Ministry of Land, Infrastructure and Transport of Korean government. This research was also supported by a grant (21SCIP-B146959-04) from Construction technology research program funded by Ministry of Land, Infrastructure and Transport of Korean government.

References

[1] Xu SH. Estimating the effects of corrosion pits on the fatigue life of steel plate based on the 3D profile. Int J Fatigue 2015;72:27–41.
[2] Biondini F, Vergani M. Deteriorating beam finite element for nonlinear analysis of concrete structures under corrosion. Struct Infrastruct Eng 2015;11(4):519–32.
[3] Li F, Luo X, Wang K, Ji Y. Pitting damage characteristics on prestressing steel strands by combined action of fatigue load and chloride corrosion. J Bridge Eng 2017;22(7):04017023.
[4] Guo T, Sause R, Frangopol DM, Li A. Time-dependent reliability of PSC box-girder bridge considering creep, shrinkage, and corrosion. J Bridge Eng 2011;16(1):29–43.
[5] AASHTO. AASHTO LRFD bridge design specifications. 8th ed. Washington, DC: AASHTO; 2017.
[6] Cho T, Kim TS. Probabilistic risk assessment for the construction phases of a bridge construction based on finite element analysis. Finite Elem Anal Des 2008;44(6–7):383–400.
[7] Huang Q, Gardoni P, Trejo D, Pagnotta A. Probabilistic model for steel–concrete bond behavior in bridge columns affected by alkali silica reactions. Eng Struct 2014;71:1–11.
[8] Liu Y, Zhang S. Probabilistic baseline of finite element model of bridges under environmental temperature changes. Comput-Aided Civ Infrastruct Eng 2017;32(7):581–98.
[9] Yang IH. Prediction of time-dependent effects in concrete structures using early measurement data. Eng Struct 2007;29(10):2701–10.
[10] Lee J, Lee Y, Kim H, Sim S, Kim J. A new methodology development for flood fragility curve derivation considering structural deterioration for bridges. Smart Struct Syst 2016;17(1):149–65.
[11] Kim H, Sim SH, Lee J, Lee YJ, Kim, JM. Flood fragility analysis for bridges with multiple failure modes. Adv Mech Eng; 2017;9(3):1687814017696415.
[12] Petrolo M, Zappino E, Carrera E. Refined free vibration analysis of one-dimensional structures with compact and bridge-like cross-sections. Thin-Walled Struct 2012;56:49–61.
[13] Toi Y, Kobashi K, Iezawa T. Finite element analysis of thermal elasto-plastic behaviours of bridge girders in hot-dip galvanization. Comput Struct 1994;53(6):1307–16.
[14] Bažant ZP, Vořechovský M, Novák D. Asymptotic prediction of energetic-statistical size effect from deterministic finite-element solutions. J Eng Mech 2007;133(2):153–62.
[15] Mihai LA, Ainsworth M. An adaptive multi-scale computational modelling of Clare College Bridge. Comput Methods Appl Mech Eng 2009;198(21–26):1839–47.
[16] Hussein HH, Walsh KK, Sargand SM, Al Rikabi FT, Steinberg EP. Modeling the shear connection in adjacent box-beam bridges with ultrahigh-performance concrete joints. I: Model calibration and validation. J Bridge Eng 2017;22(8):04017043.
[17] Qin S, Zhou YL, Cao H, Wahab MA. Model updating in complex bridge structures using kriging model ensemble with genetic algorithm. KSCE J Civ Eng 2018;22(9):3567–78.
[18] Wu J, Yan Q, Huang S, Zou C, Zhong J, Wang W. Finite element model updating in bridge structures using Kriging model and Latin hypercube sampling method. Adv Civ Eng 2018;2018.
[19] Zhang Y, Wu G. Seismic vulnerability analysis of RC bridges based on kriging model. J Earthquake Eng 2019;23(2):242–60.
[20] Lee J, Lee YJ, Shim CS. Probabilistic prediction of mechanical characteristics of corroded strands. Eng Struct 2020;203:109882.
[21] Myers RH, Montgomery DC, Anderson-Cook CM. Response surface methodology: process and product optimization using designed experiments. John Wiley & Sons; 2016.
[22] Rasmussen CE, Williams CK. Gaussian processes for machine learning. Cambridge, USA: MIT press; 2006.
[23] Melchers RE. Structural reliability analysis and prediction. John Wiley & Sons; 2018.
[24] Liu PL, Der Kiureghian A. Multivariate distribution models with prescribed marginals and covariances. Probab Eng Mech 1986;1(2):105–12.
[25] Ang AHS, Tang WH. Probability concepts in engineering planning and design: Emphasis on application to civil and environmental engineering. Wiley; 2007.
[26] Darmawan MS, Stewart MG. Effect of pitting corrosion on capacity of prestressing wires. Mag Concr Res 2007;59(2):131–9.
[27] Ebeling RM, White BC, Evans JA, Haskins RW, Miller EL. Corrosion Induced Loss of Capacity of Post Tensioned Seven Wire Strand Cable Used in Multistrand Anchor Systems Installed at Corps Projects. ARMY ENGINEER WATERWAYS EXPERIMENT STATION VICKSBURG MS VICKSBURG United States; 2016.
[28] Jeon CH, Lee JB, Lon S, Shim CS. Equivalent material model of corroded prestressing steel strand. J Mater Res Technol 2019;8(2):2450–60.
[29] Jeon CH, Nhuyen CD, Shim CS. Assessment of mechanical properties of corroded prestressing strands. Appl Sci 2020;10(12):4055.
[30] Rosenblatt M. Remarks on some nonparametric estimates of a density function. Ann Math Stat 1956:832–7.
[31] Parzen E. On estimation of a probability density function and mode. Ann Math Stat 1962;33(3):1065–76.
[32] British Standards Institution. Eurocode 2: Design of concrete structures: Part 1-1: General rules and rules for buildings. British Standards Institution; 2004.
[33] Bae BI, Choi HK, Lee BS, Bang CH. Compressive behavior and mechanical characteristics and their application to stress-strain relationship of steel fiber-reinforced reactive powder concrete. Adv Mater Sci Eng 2016;2016.
[34] CEB. High Performance Concrete, Bulletim d'Information, Lausanne, Switzerland, 1995;228(60).